DOI: 10.19884/j.1672-5220.202503014

Numerical Simulation of Bowing Distortion Formation of BOPET Film During Tentering Process

PAN Hongzhou, WU Shiqi, YANG Shenglin*
College of Materials Science and Engineering, Donghua University, Shanghai 201620, China

Abstract: When preparing biaxially oriented polyethylene terephthalate (BOPET) films through sequential biaxial stretching, bowing distortion occurs within the film plane, leading to inhomogeneous optical and mechanical properties between the edge and central regions of the films. This quality degradation renders the films unsuitable for optical applications. Considering that polyethylene terephthalate (PET) macromolecules are in a rubbery state and have crystalline physical crosslinking points when the film is stretched above its glass transition temperature T_g but below the melting point T_m, this study establishes a visco-hyperelastic model. The model parameters are obtained by numerically fitting the experimental results of uniaxial stretching and stress relaxation tests. These fittings yield the second-order coefficient of the Mooney-Rivlin polynomial (describing hyperelasticity) and the third-order coefficient of the Prony series (describing viscosity). Then, ANSYS finite element simulations of the tentering process of PET films are carried out with the isotropic elastic, the orthotropic elastic, the plastic, and the visco-hyperelastic material models, respectively. The simulated bowing distortion obtained from the visco-hyperelastic model shows better agreement with experimental results, demonstrating that this model can accurately capture the mechanical response behavior of PET films during biaxial stretching.

Keywords: biaxially oriented polyethylene terephthalate (BOPET) film; tentering process; bowing distortion; visco-hyperelastic model; numerical simulation
CLC number: TQ323.41 **Document code**: A
Article ID: 1672-5220(2026)04-0034-07

0 Introduction

Biaxially oriented polyethylene terephthalate (BOPET), known as a paramount polymeric film material combining optical clarity, mechanical strength, and chemical resistance, finds extensive application in packaging, magnetic recording media, electrical insulation, synthetic paper, reprographic systems, and flat panel displays. Commercial BOPET production typically involves sequential stages: melt casting, machine direction (MD) stretching, transverse direction (TD) stretching, thermosetting, edge trimming, and winding. Normally, MD stretching is first conducted between differential speed rollers, followed by TD stretching and thermosetting in a tenter frame, where the dual chain clamps drive the polyethylene terephthalate (PET) sheet to move along the MD as well as drag the two edges of the sheet away from each other. During the tentering process, bowing distortion often emerges in the polymer film.

Bowing distortion refers to the discrepancy between the direction of the molecular orientation axis at the center and the edge of the film width, and causes the mechanical and optical anisotropies in the film. Bowing phenomena, just as originally reported by Kase et al.[1] and Sakamoto[2], mainly originate from Poisson's compression of polymer sheets undergoing TD stretching. Further studies have shown that the causes of bowing distortion are rather complex and are associated with the stretching temperature and rate[3-5], the stretching ratio compatibility between MD and TD[6], as well as the material property, i.e., the microstructure or composition of the polymer base[7-10]. Yamada et al.[11] and Tokihisa et al.[12] have investigated the deformation behavior of polymer films during the tentering process by means of numerical simulations and attempted to reduce the bowing distortion based on the comparison of the numerical and experimental results[13].

Till now, the material models used to numerically analyze the tentering process of polymer films have mainly been elastic ones[11], as researchers intend to reduce the risk of computational divergence. However, real polymer materials show complex time-dependent plastic behavior when subjected to a history of stress or strain. To approximate the features of this behavior, a viscoelastic model should be adopted. The viscoelastic model commonly exhibits a proper combination of an elastic component, which reflects the instantaneous response, and a viscous component, which represents the relaxation of the polymer.

Moreover, concerning the viscoelasticity of the PET film, the underlying elasticity should be chosen as

Received date: 2025-03-14
* Correspondence should be addressed to YANG Shenglin, email: slyang@dhu.edu.cn
Citation: Pan H Z, Wu S Q, Yang S L. Numerical simulation of bowing distortion formation of BOPET film during tentering process [J]. *Journal of Donghua University (English Edition)*, 2026, 43(4): 34-40.

hyperelasticity for two reasons. First, during the tentering process, the film will be subjected to a large deformation (or large strain). Therefore, a hyperelastic constitutive equation should be used to maintain the accuracy of numerical computation. Second, PET itself acts as a rubbery material under the stretching temperature (usually above the glass transition temperature T_g, while below the melting point T_m). PET is one of the crystalline polymers, and it can be reasonably expected that PET film will crystallize when stretched at a temperature above T_g. Therefore, there are both permanent crosslinks (the crystallites) and physical entanglements (the sliplinks) of the molecular chains within PET, just as described by Edwards et al.[14] and Long et al.[15]. These crosslinks will impart "rubber elasticity" to the film to some extent. Apparently, the crosslink density is relevant to the crystallinity. Therefore, if using the hyperelastic concept in finite element (FE) analysis, we can incorporate an observable quantity (the crystallinity) into the computation model, which undoubtedly can improve the comparability of the model with real conditions.

In this study, the FE analysis on the tentering process of PET film has been carried out via ANSYS based on several material models, i. e., the isotropic elastic, the orthotropic elastic, the plastic, and the visco-hyperelastic material models. All material models were established through fitting the experimental data of a series of mechanical tests of PET film samples. Subsequently, the calculated bowing distortions from those models were compared with the experimental testing data, and the accuracy of those models in reflecting the mechanical behavior of PET was discussed.

1 Materials and Methods

1.1 Materials

In the present study, the material models of PET used in the FE simulation are obtained through curve fitting of experimental testing data of PET samples in various mechanical tests.

Sample Ⅰ is the amorphous PET sheet with a thickness of 530 μm cast at 275 ℃ from the raw material (FG604) supplied by Sinopec Yizheng Chemical Fiber Co., Ltd., China. Sample Ⅱ is the uniaxially stretched Sample Ⅰ along the MD with a series of differential speed rollers at a stretching temperature of 87 ℃, a stretching ratio of 2.4, and a line speed of 7.3 m/min. Sequentially, Sample Ⅱ is further stretched along the TD at a stretching temperature of 100 ℃, a stretching ratio of 3.8, and a line speed of 5.0 m/min in a tenter frame. Then, the machine is shut down, and the whole specimen from the inlet to the outlet of the tenter frame is picked out immediately and designated as Sample Ⅲ.

1.2 Measurement of bowing distortion

The tentering process of BOPET film is demonstrated in Fig. 1(a), where the red line marks Sample Ⅲ. The uniaxially stretched PET film (Sample Ⅱ) is transversely stretched, and the previously marked parallel lines will transform into an arch shape, just as demonstrated in Fig. 1(b). For each arch line, if taking the deviation of the apex point as b (positive b represents left bending while negative b represents right bending) and the chord length as W, the bowing distortion B is defined as

$$B = b/W. \tag{1}$$

The bowing distortion distribution along MD is recorded for Sample Ⅲ, which will be compared with the numerical simulation results.

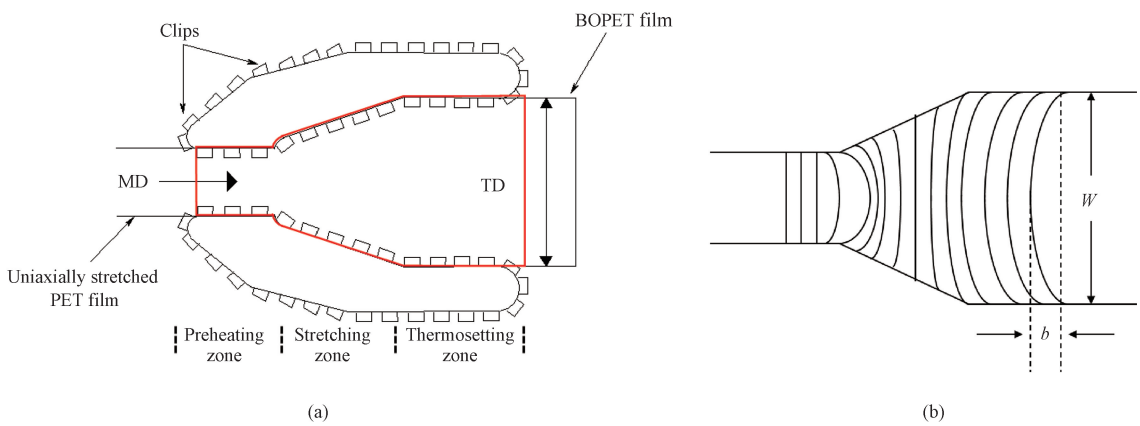


Fig. 1 Diagram of tentering process and bowing distortion of BOPET film: (a) tentering process; (b) bowing distortion

1.3 Mechanical test of PET samples

The amorphous PET sheet (Sample Ⅰ) was uniaxially stretched with a lab-built tensile testing machine at different temperatures (75–120 ℃ with a step of 15 ℃) and different speeds (1%/s–9%/s with a step of 2%/s).

Sample Ⅱ was uniaxially stretched with the equipment mentioned above along a direction

perpendicular to MD (i.e., TD) at different temperatures (75–120 ℃ with a step of 15 ℃) and different speeds (1%/s–9%/s with a step of 2%/s).

The stress relaxation behavior of the PET film was characterized by recording the stress varying over time of Sample Ⅱ after being applied a step strain (applied at a rapid speed of 100%/s) of 5% along TD at different temperatures (75–120 ℃ with a step of 15 ℃).

1.4 Establishment of material models of PET

The results of the mechanical tests in Subsection 1.3 were input into the material properties module of ANSYS software and fitted under different material models to obtain the mechanical constants.

1.5 FE simulation

The tentering process of the uniaxially stretched PET film can be approximately modeled as a two-dimensional plane stress problem. Because of the symmetry of the problem, only half of the film needs to be analyzed. Figure 2 describes the dimension of the problem, where rectangle *ABCD* (size: $HW \times L$) stands for the half part of the untentered film, and after a tentering with a draw ratio of *DR*, the shape of the film will change to be a polygon *ABCEFG*; the line speed (machine speed) is *VM* and the tentering speed is *VT* (if the dimension of a real pilot plant is fixed, *VT* should be decided by *VM*).

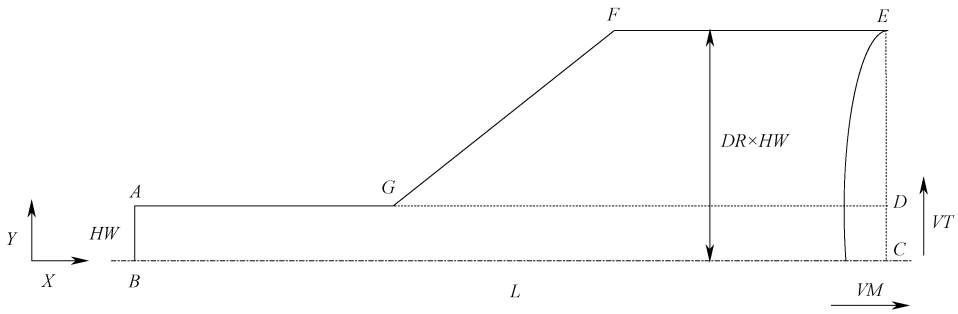


Fig. 2 Dimensions of FE simulation of PET film under tentering process

The numerical simulation of the PET film tentering process is carried out by using ANSYS, in which the element type is chosen as PLANE182, and the boundary conditions of *ABCD* are set as follows.

Left edge *AB*: all degrees of freedom (DOFs) are restricted.

Bottom edge *BC*: symmetry boundary condition (B.C.) is imposed.

Right edge *CD*: free boundary.

Upper edge *DA*: *UX* is fixed at zero ($UX = 0$), corresponding to the film clamped by tentering clips.

Moreover, the load (displacement *UY* of edge *DA*) changes with the calculation time (independent variable $\{TIME\}$) and the position of the nodes in line *DA* (coordinate $\{X\}$), which can be presented by an ANSYS function:

$$UY = VT \times \min(\max(0, \{M1\}), M0),$$

in which

$$M0 = (DR - 1) \times HW/VT$$

represents the time needed to reach maximum displacement in the *Y* direction while

$$M1 = \{TIME\} - (L - \{X\})/VM$$

is defined to ensure that the displacement will happen just in line *EFG*, whereas line *GA* remains unchanged. Furthermore, such a defined load ensures a tentering deformation that first happens at point *D* and transfers to the left along *DA* gradually. During the simulation, the free variables mentioned above are chosen as

$$HW = 0.1 \text{ m},$$
$$L = 10 \text{ m},$$
$$VM = 0.075 \text{ m/s},$$
$$VT = 0.005 \text{ m/s},$$
$$DR = 3.8.$$

It should be noted that the tentering of the PET film is not an isothermal process, and the tenter frame is usually divided into three temperature zones, namely the preheating zone, stretching zone, and thermosetting zone. In this simulation, the temperature conditions were chosen as follows (Fig. 3).

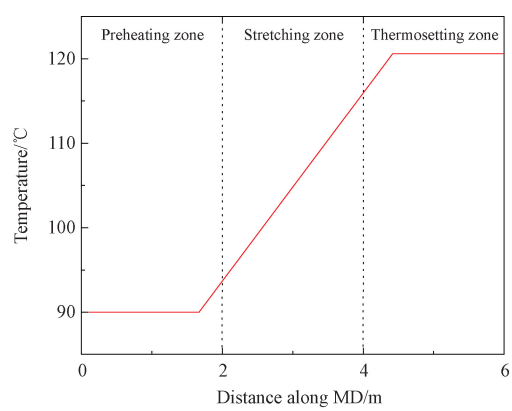


Fig. 3 Temperature condition during FE simulation

Moreover, the mechanical constants used in FE simulation will vary with respect to the temperature, which is just a linear interpolation process automatically performed by ANSYS if the experimental data at different

temperatures have been provided.

2 Results and Discussion

2.1 Material models of PET

1) Isotropic elastic model

The true stress-true strain curve of the amorphous PET sheet under uniaxial stretching is shown in Fig. 4 (for clarity, only the data obtained at 105 ℃ are listed and the same below), where PET acts as a typical plastic material. However, when considering the stability of FE calculations and using an elastic model, the curve in Fig. 4 can be linearly fitted. The slope obtained from the fitting is the isotropic elastic modulus *EX*. Hereafter, the mechanical constants are given without units but corresponding to the SI unit system of ANSYS.

$$EX = 47.9E6.$$

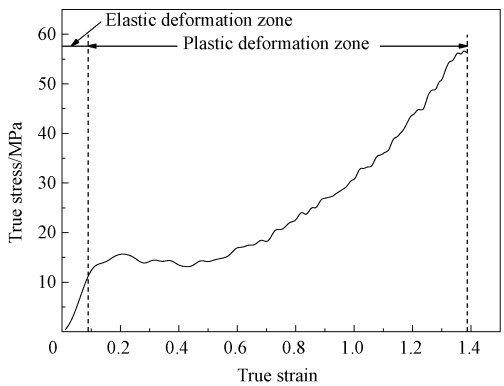


Fig. 4 True stress-true strain curve of amorphous PET sheet under uniaxial stretching

2) Orthotropic elastic model

The PET macromolecules orient along the stretching direction. Therefore, the uniaxially stretched PET film, such as Sample Ⅱ, possesses different mechanical responses along the stretching direction and its perpendicular direction, showing an orthotropic behavior. If deducing the TD elastic modulus from the transverse stretching data of Sample Ⅱ (Fig. 5(a)) by using the same scheme mentioned above, and estimating the MD elastic modulus to be the same as the isotropic elastic modulus *EX*, the orthotropic elastic modulus *EY* of PET can be described as

$$EX = 47.9E6,$$

$$EY = 7.98E6.$$

3) Plastic model

The plastic behavior of PET demonstrated in Fig. 4, namely the relationship of stress σ and strain ε, can be approximated by a nonlinear function

$$\sigma = k + R_0\varepsilon + R_\infty(1 - \exp(-\beta\varepsilon)),$$

where k, R_0, R_∞, and β are constants and can be determined by curve fitting as

$$k = 12 \times 10^6,$$

$$R_0 = 25.95 \times 10^6,$$

$$R_\infty = 6.86 \times 10^{-6},$$

$$\beta = 7.29 \times 10^{-5}.$$

4) Visco-hyperelastic model

To describe the hyperelastic behavior of a certain material, the so-called Mooney-Rivlin strain energy potential U can then be defined as

$$U = U(\bar{I}_1, \bar{I}_2, J) = U(\bar{\lambda}_1, \bar{\lambda}_2, \bar{\lambda}_3, J),$$

where $\bar{I}_1$ and $\bar{I}_2$ are the invariants of the deformation tensor; $\bar{\lambda}_1$, $\bar{\lambda}_2$, and $\bar{\lambda}_3$ are the eigenvalues of the deformation tensor; J is the product of the three eigenvalues of the deformation tensor. Especially, the second order of the Mooney-Rivlin model is

$$U = C_{10}(\bar{I}_1 - 3) + C_{01}(\bar{I}_2 - 3) + \frac{1}{d}(J - 1)^2,$$

where C_{10}, C_{01}, and d are material constants, and can be obtained by curve fitting of the transverse stretching data of Sample Ⅱ through the relationship:

$$\mu = 2(C_{10} + C_{01}),$$

$$K = \frac{2}{d},$$

where μ is the initial shear modulus; K is the initial bulk modulus. They are related to the elastic modulus E via

$$E = 2\mu(1 + \nu) = 3K(1 - 2\nu),$$

where ν is the Poisson's ratio.

Concerning the viscosity of polymer materials, the Maxwell spring-dashpot model is usually utilized to describe the microstructures of the polymer, implying that the response of the polymer to a mechanical load is a relaxation process. Therefore, the viscosity of the PET film can be demonstrated by the stress relaxation testing, which can further be fitted with a time-dependent exponential decay series (Prony series):

$$y = y_\infty + \sum_{i=1}^{n} y_i \exp\left(-\frac{x}{\tau_i}\right),$$

where y stands for the total stress; y_∞ stands for the equilibrium stress at infinite time; y_i stands for the stress of the ith spring-dashpot unit; x stands for the time; τ_i stands for the intrinsic relaxation time of the ith spring-dashpot unit. The experimental data of the uniaxial stretching and the stress relaxation for Sample Ⅱ are listed in Fig. 5. After curve fitting calculations, ANSYS gives the following coefficients for the Mooney-Rivlin polynomials:

$$C_{10} = -0.83 \times 10^8,$$

$$C_{01} = 1.10 \times 10^8,$$

$$d = 0.17 \times 10^{-7},$$

and the Prony series:

$$y_\infty = 1.489 \times 10^6,$$

$$y_1 = 9.256 \times 10^6,\ \tau_1 = 1.226,$$

$$y_2 = 3.727 \times 10^6,\ \tau_2 = 20.24,$$

$$y_3 = 1.515 \times 10^6,\ \tau_3 = 305.1.$$

The reproduced fit functions obtained from those coefficients are also drawn in Fig. 5, and it can be found that they coincide well with the experimental data.

In general, the measurement of Poisson's ratio ν is rather difficult. Nevertheless, considering that PET is in a rubbery state at the stretching temperature T, a first-order polynomial

$$\nu = 0.1 + 2.67 \times 10^{-3} T$$

could be chosen to estimate the temperature dependence of Poisson's ratio (if the temperature changes from 90 to 120 ℃, ν will increase from 0.34 to 0.42) in the FE simulation.

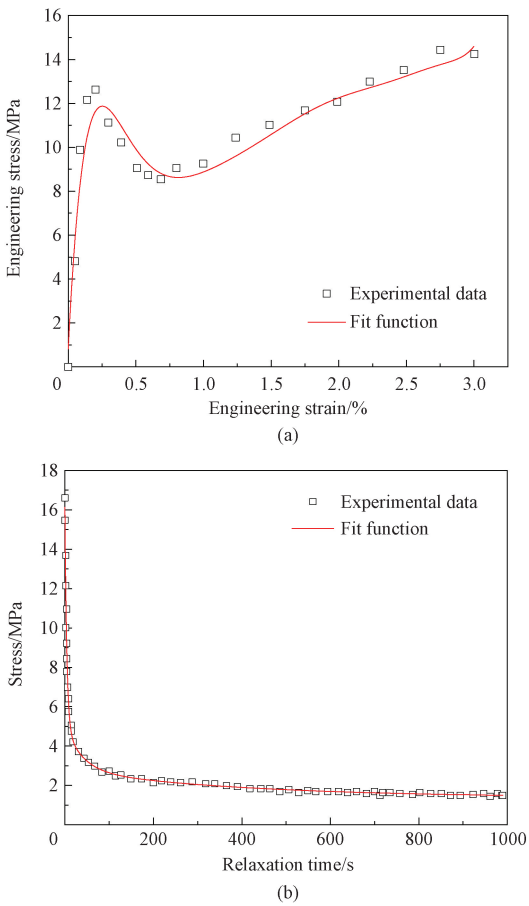


Fig. 5 Test results of Sample Ⅱ and their fit functions: (a) uniaxial stretching; (b) stress relaxation

2.2 FE simulation of tentering process of PET film

The FE simulation in this study involves large deformation and highly nonlinear material models. It is found that the FE calculation can be completed rapidly and shows good convergence for the isotropic and orthotropic elastic models. However, fairly small time steps (10^{-4} – 10^{-6}) must be set for the plastic and visco-hyperelastic material models to maintain computing stability and convergence.

Figure 6 shows the evolution of deformation of the FE model and the distribution of the X component displacement obtained from the visco-hyperelastic model. In each contour subplot, MX and MN denote locations of maximum and minimum X component displacement, respectively. From top to bottom, the calculation time increases by an interval of 1. According to the definition listed in Eq. (1), the distribution of bowing distortion B along the MD can be calculated from the numerical simulation of different PET material models, which is demonstrated in Fig. 7. Moreover, the bowing distortions measured from Sample Ⅲ are also listed in Fig. 7. It is found that simulated bowing distortions calculated by the visco-hyperelastic model show the best fit to experimental data, compared with results from isotropic elastic, orthotropic elastic and plastic models. In particular, the visco-hyperelastic model can better reflect the trend of the actual bowing distortion in the thermosetting zone.

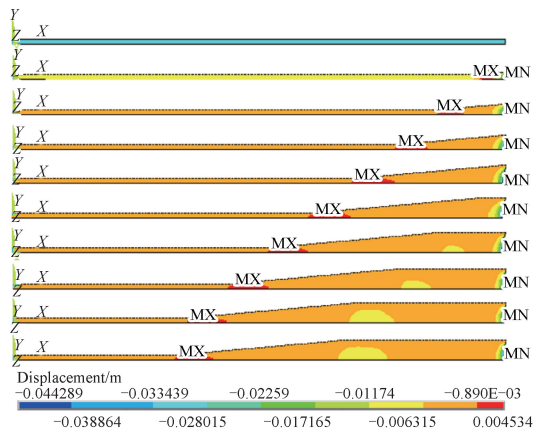


Fig. 6 Contour maps of X component displacement of FE model for PET film undergoing tentering process

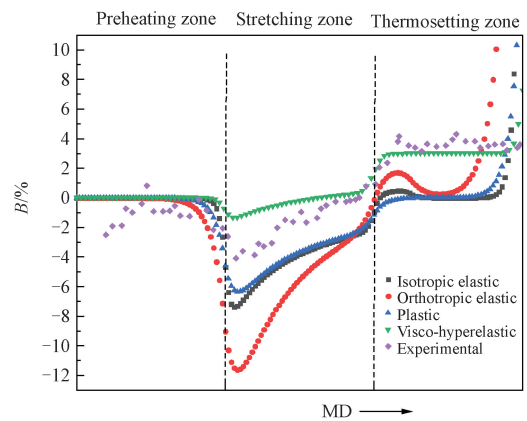


Fig. 7 Distribution of bowing distortion along MD

3 Conclusions

This study used experimental data from uniaxial tension and stress relaxation to establish hyperelastic and viscous models through fitting methods and combined the two as material models. The finite element simulation of the PET stretching process was carried out using ANSYS, and the simulated bowing distortion matched well with experimental results, indicating that the visco-hyperelastic model can accurately reflect the mechanical behavior of PET, superior to other material models such as isotropic elastic, orthotropic elastic, and plastic models.

References

[1] Kase S, Nishimura T. Extension of plane rubber films[J]. *Journal of Rheology*, 1990, 34(2): 251-273.

[2] Sakamoto K. Effects of stretching conditions on thickness distribution in biaxially stretched polypropylene films[J]. *Journal of the Japan Society of Polymer Processing*, 1991, 3: 496-503. (in Japanese)

[3] Makke A, Lame O, Perez M, et al. Nanoscale buckling in lamellar block copolymers: a molecular dynamics simulation approach[J]. *Macromolecules*, 2013, 46(19): 7853-7864.

[4] Kawakami D, Hsiao B S, Burger C, et al. Deformation-induced phase transition and superstructure formation in poly (ethylene terephthalate)[J]. *Macromolecules*, 2005, 38(1): 91-103.

[5] Kitamura Y, Okada K, Masunaga H, et al. Role of strain rate in the strain-induced crystallization (SIC) of natural and synthetic isoprene rubber[J]. *Polymer Journal*, 2019, 51(2): 221-226.

[6] Dechnarong N, Kamitani K, Cheng C H, et al. In situ synchrotron radiation X-ray scattering investigation of a microphase-separated structure of thermoplastic elastomers under uniaxial and equi-biaxial deformation modes[J]. *Macromolecules*, 2020, 53(20): 8901-8909.

[7] Shen J, Sugimoto I, Matsumoto T, et al. Fabrication and characterization of elastomeric semiconductive thiophene polymers by peroxide crosslinking[J]. *Polymer Journal*, 2019, 51(2): 257-263.

[8] Ishige R. Precise structural analysis of polymer materials using synchrotron X-ray scattering and spectroscopic methods[J]. *Polymer Journal*, 2020, 52(9): 1013-1026.

[9] Nishitsuji S, Watanabe Y, Takebe T, et al. X-ray scattering study on the changes in the morphology of low-modulus polypropylene under cyclic uniaxial elongation[J]. *Polymer Journal*, 2020, 52(3): 279-287.

[10] Rahmawati R, Masuda S, Cheng C H, et al. Investigation of deformation behavior of thiourethane elastomers using in situ X-ray scattering, diffraction, and absorption methods[J]. *Macromolecules*, 2019, 52(18): 6825-6833.

[11] Yamada T, Nonomura C, Matsuo T. Analyses of bowing phenomena in successive transverse stretching and thermosetting process for biaxially oriented film[J]. *International Polymer Processing*, 1995, 10(4): 334-340.

[12] Tokihisa M, Kushizaki Y, Tomiyama H, et al. The prediction of bowing distortion of film after transverse stretching with consideration of heated air flow in a tenter[J]. *International Polymer Processing*, 2011, 26(5): 498-507.

[13] Yamada T, Nonomura C. Attempt to reduce bowing distortion in tentering of film[J]. *Journal of Applied Polymer Science*, 1994, 52: 1393-1403.

[14] Edwards S F, Vilgis T. The effect of entanglements in rubber elasticity[J]. *Polymer*, 1986, 27(4): 483-492.

[15] Long S D, Ward I M. Shrinkage force studies of oriented polyethylene terephthalate[J]. *Journal of Applied Polymer Science*, 1991, 42(7): 1921-1929.

双向拉伸聚酯膜张幅过程中弯曲畸变形成的数值模拟

潘泓舟，吴诗颀，杨胜林*
东华大学 材料科学与工程学院，上海 201620

摘　要：采用逐步双向拉伸制备双向拉伸聚酯膜时，膜平面内会产生弯曲畸变，导致膜边缘和中间部分的光学、力学等性能不均一，膜品质劣化而不能顺利应用于光学产品领域。聚酯膜在高于玻璃化转变温度而低于熔点的拉伸温度下，大分子处于高弹态，且存在由结晶形成的物理交联点。基于该特点，本研究通过对聚酯膜单向拉伸及应力松弛试验结果分别进行拟合，确定模型参数，得到了描述超弹性的 Mooney-Rivlin 多项式的 2 阶系数及描述黏性的 Prony 级数的 3 阶系数，从而建立了聚酯膜的黏性–超弹模型。分别采用各向同性弹性、正交各向异性弹性、塑性及黏性–超弹四种材料模型，借助 ANSYS 软件对聚酯膜的张幅过程进行有限元模拟。计算结果表明由黏性–超弹模型得到的弯曲畸变与试验数据吻合度较高，说明该材料模型能够较准确地反映聚酯膜在双向拉伸过程中的力学响应行为。

关键词：双向拉伸聚酯膜；张幅加工；弯曲畸变；黏性–超弹模型；数值模拟